

Ultrafast vibrational relaxation of diatomic chalcogen hydrides in alkali halides

C. E. Mungan,^{a)} U. Happek,^{b)} J. T. McWhirter,^{c)} and A. J. Sievers

Laboratory of Atomic and Solid State Physics and Materials Science Center, Cornell University, Ithaca, New York 14853-2501

(Received 21 March 1997; accepted 5 May 1997)

The energy relaxation times of the fundamental stretching modes in the electronic ground state of OH^- , OD^- , SH^- , and TeH^- in a variety of alkali halides are measured by incoherent laser saturation and found to vary from 0.3 to 3 ns at 1.7 K. These vibrational lifetimes are between 4 and 8 orders of magnitude smaller than those of other heteronuclear diatomics diluted in crystals, including the ionic systems of CN^- in salts and the neutral deuterides, DCl and ND, and oxides, CO and NO, in rare-gas matrices. Unlike these other systems, the chalcogen-hydride-doped alkali halides have a librational mode at frequencies well above the top of the host phonon band. This makes the librational decay channel a lower order process than relaxation into phonons. An energy gap law can be fit to the data, in which the relaxation times vary exponentially with the number of accepting reorientational modes. This model can explain the fact that OH^- and OD^- in KCl have nearly the same lifetimes, since the vibrational and librational frequencies both have the same isotope shift. Furthermore, previous persistent spectral hole burning measurements of SH^- in mixed crystals are consistent with a picture in which the defects reorient during vibrational de-excitation. It is found that the reorientational decay rates are much faster than the equal-decay-order relaxation of CN^- into translational modes in the silver and sodium halides. This could be explained by a factor of ~ 3 enhancement in the vibrational coupling constant to reorientations as compared to translations, but the relative strengths of the appropriate sidebands do not appear to support such an enhancement. The relaxation times of the diatomic hydrides are also found to be much smaller in ionic than in van der Waals hosts, even for equal order reorientational relaxation, suggesting that Coulombic forces significantly increase the V - R coupling strength. © 1997 American Institute of Physics. [S0021-9606(97)00231-6]

I. INTRODUCTION

At low concentrations in a crystalline lattice, a diatomic molecular impurity whose internal vibrational mode is high in frequency relative to the host phonon bands is generally expected to decay radiatively at low temperatures, since non-radiative multiphonon relaxation constitutes a large order process. This expectation is borne out for CO, NO, CN, DCl, and ND in rare-gas matrices,¹⁻⁶ as well as for CN^- in the potassium, rubidium, and cesium halides.^{7,8} For two of these molecules, laser emission has been obtained on the vibrational transitions.^{9,10} In contrast, recent preliminary measurements¹¹ of the vibrational relaxation of OH^- and SH^- in the potassium halides indicate lifetimes on the order of 1 ns, much shorter than the radiative limit of ~ 50 ms. This agrees with the experimentally determined upper limit of 5 ns on the SH^- nonradiative lifetime, deduced from the lack of $2 \rightarrow 1$ vibrational fluorescence following $0 \rightarrow 2$ overtone pumping.¹² These results are surprising, since the stretching modes of these hydrides are higher in frequency than those of these other systems, and hence a higher order multiphonon relaxation process is anticipated.

An alternative nonradiative decay channel open to select systems is vibrational relaxation into rotations of the impurity molecule. Such a model was first proposed in 1975, for the vibrational relaxation of OH and OD in crystalline Ne at 4.2 K—the relaxation rate was found to be 2.3 times *faster* for the hydride than for the deuteride.¹³ This contradicts a multiphonon-relaxation model, and it was proposed that the decay is into nearly free rotations instead. Matching the vibrational transition frequency, ν_{01} , to the rotational energy requires $\nu_{01} = BJ(J+1)$, where B is the rotational constant and J is the rotational quantum number of the accepting level. Neglecting the factor of 1, since the rotational quantum number is large, gives

$$J \approx \sqrt{\nu_{01}/B} \quad (1)$$

(with a host phonon taking up the difference in the event that the right-hand side is nonintegral). But the stretching frequency is proportional to the inverse square root of the reduced mass, μ , of the molecule, whereas the rotational constant is proportional simply to the reciprocal of μ via the moment of inertia. Hence, $J \propto \mu^{1/4}$ and OD is predicted to be a $\sim 20\%$ higher order process than OH, explaining its slower relaxation. Similar measurements and conclusions were made for NH and ND in Ne, Ar, and Kr.^{6,14} The vibrational

^{a)}Present address: Dept. of Physics, University of West Florida, Pensacola, FL 32514.

^{b)}Present address: Dept. of Physics and Astronomy, University of Georgia, Athens, GA 30602.

^{c)}Present address: Dept. of Physics, Union College, Schenectady, NY 12308.

relaxation of HCl, which exhibits weakly hindered rotations,^{15,16} has been measured for levels up to $\nu=3$ and is inconsistent with a multiphonon scheme; relaxation into local modes, such as rotations, is proposed instead.^{5,17}

In the present paper, a comprehensive study of the vibrational relaxation at low temperatures and concentrations of the diatomic chalcogen hydrides in the alkali halides is reported. In addition to extending the afore-mentioned OH⁻ and SH⁻ measurements to several additional hosts, new results are presented for OD⁻ and TeH⁻. A total of 11 different systems are measured and the vibrational relaxation times, T_1 , are found to vary from 0.3 to 3 ns. The lack of a significant OH⁻ isotope effect in the relaxation time upon deuteration, in particular, rules out a multiphonon-decay model, as the deuterated species is a factor of 1.36 (approximately $\sqrt{2}$) closer in frequency to the host phonon bands than is the hydride, and hence its relaxation process would be that much lower in order. Assuming that the vibration-to-phonon coupling constants for the two isotopes are identical, one would then have expected an exponentially faster decay rate for OD⁻ compared to OH⁻, in contrast to experiment. On the other hand, spectroscopic measurements indicate the existence of a superoptic local mode, identified as a librational mode of the molecule about its center of mass.¹⁸⁻²⁰ An energy gap law is found to describe the relaxation of the vibrations into these reorientational modes, using one set of coupling constants for all of the chalcogen hydrides. The $\sqrt{2}$ reduction in the hydroxide librational frequency upon deuteration, identical to the reduction in the vibrational frequency, then explains the observed null isotope effect in the lifetime.

The outline of the paper is as follows. In Sec. II, incoherent laser saturation measurements are outlined in detail. Beginning with the experimental setup, data are presented for a number of different systems. An appendix describes how the energy relaxation times are extracted from these data. In Sec. III, theoretical models for the vibrational decay into host lattice phonons or local reorientational modes are compared with the experimental results. In the next section, the results are discussed in the light of previous experiments. Finally, Sec. V concludes with a brief summary.

II. VIBRATIONAL SATURATION MEASUREMENTS

A. Experimental setup

Incoherent laser saturation is used to measure the vibrational lifetimes of the isolated chalcogen hydrides, XH⁻, in the alkali halides. While the concept behind the method is straightforward,²¹⁻²³ it suffers from the drawback that the analysis depends on a significant number of optical and material parameters which must be separately determined, thus limiting the absolute accuracy. However, the more direct technique of pump-probe spectroscopy is not currently practical, since present picosecond laser systems do not simultaneously support the requisite high pulse energies, narrow spectral bandwidth, and frequency tunability.

The experimental apparatus is sketched in Fig. 1. The Nd³⁺:YAG laser is Q switched, delivering 1.1 J pulses with

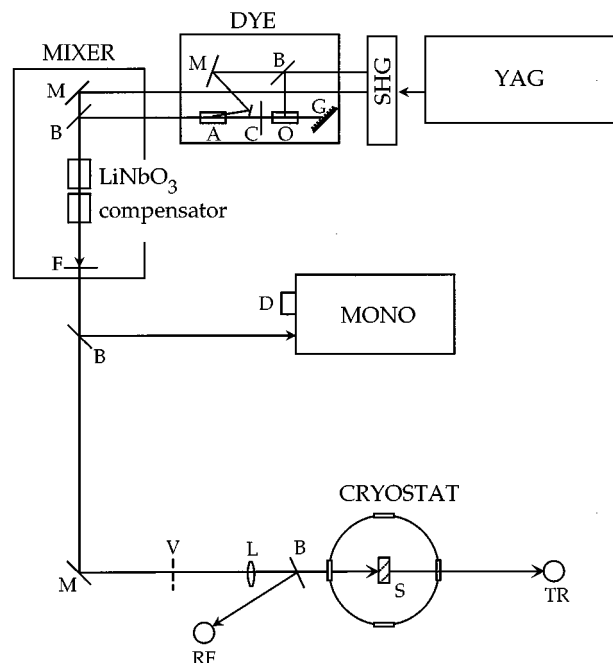


FIG. 1. Experimental setup (not to scale) for laser saturation measurements. The indicated components are as follows: YAG—Q-switched Nd³⁺:YAG laser; SHG—second harmonic generator and frequency separator: the upper beam leaving this unit is the 532 nm pulse train and the lower is the residual 1.064 μm fundamental; DYE—dye-laser system: the 532 nm pulses pump an oscillator (O) dye cell, in a cavity composed of a grating (G) and an output coupler (C), as well as two single-pass amplifier (A) dye cells, only one of which is shown; MIXER—optical-frequency-mixing module: the residual fundamental and dye laser beams are combined and difference-frequency mixed in a LiNbO₃ (or LiIO₃) crystal; the compensator is a piece of equal-length sapphire; the filter (F) is a piece of silicon at Brewster's angle which blocks any residual dye radiation and most of the residual fundamental; MONO—3/4 m monochromator for diagnostic purposes. The other labeled components are as follows: B—beamsplitter; M—mirror or prism; D—infrared detector; V—variable attenuator; L—CaF₂ lens; CRYSTAT—four-window variable-temperature cryostat; S—sample; RF and TR—PbSe detectors mounted on integrating spheres.

a width of 7–9 ns at a repetition rate of 10 Hz. An intracavity étalon reduces the bandwidth to 0.2 cm^{-1} . The beam is then frequency doubled into the green using a KD*P crystal and spatially separated from the residual fundamental. The doubled beam pumps a near-infrared dye laser. Finally, the dye radiation and the residual YAG fundamental are difference frequency mixed in either a LiNbO₃ or LiIO₃ crystal, depending on the desired wavelength. The output midinfrared pulses are 6 ns FWHM with an assumed Gaussian temporal profile, as measured using a cryogenic GaP:N photodiode. The spectral profile is also assumed to be Gaussian and has a FWHM of 0.27 cm^{-1} , determined using a 3/4 m monochromator. The pulse energies range up to $\sim 400 \mu\text{J}$, although they are considerably lower at the longest wavelengths of interest. The ir beam is linearly polarized, and is assumed to be well described by Gaussian optics near the focus at the sample. The spatial profile is measured after each run by scanning a razor blade both horizontally and vertically through the focal spot and is typically found to be 100 μm FWHM.

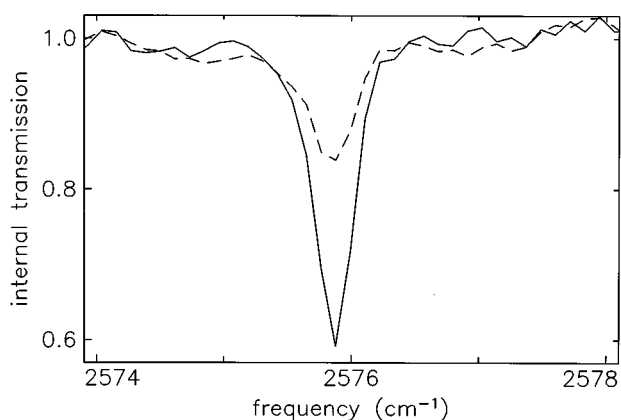


FIG. 2. Transmission of the $^{32}\text{SH}^-$ stretching mode of nominally KBr+100 ppm KSH at a bath temperature of 1.7 K for incident laser intensities of 0.1 MW/cm² (solid curve) and 150 MW/cm² (dashed curve). The internal transmission is measured by ratioing the TR and RF signals (cf. Fig. 1) and scaling the resulting background to unity. The linewidths are limited by the laser bandwidth.

The samples are suspended in a liquid-helium cryostat which is temperature controllable down to 1.7 K. Precision pinholes are used to insure coincidence of the sample mid-positions with the optical focus and corrections are made to account for the varying sample lengths. The incident intensity is attenuated using a variable neutral-density filter, and the signal is measured both before and after the cryostat using identical RT PbSe detectors mounted on integrating spheres. Filters are placed before the detectors when necessary to maintain linearity of their responses. A typical run consists in recording the averaged ratio of these two signals as a function of the incident intensity. The latter is calibrated using an energy meter, after correcting for reflection losses at the windows and front surface of the sample. The laser is tuned into resonance with the 0→1 vibrational transition by sweeping the dye-laser grating and monitoring the transmission. Since the 1→2 frequency is anharmonically shifted down in value by an amount $2x_e\nu_e$ (e.g., $\sim 100\text{ cm}^{-1}$ for²⁴ SH⁻) which in all cases is much larger than the laser bandwidth, the overtones can be ignored and the samples modeled as two-level systems. ($V-V$ transfer is negligible for the low concentrations and ultrafast relaxations of interest.⁹) At low intensities, the transmission is determined by the peak absorption coefficient of the sample, approximately reduced by the ratio of the laser bandwidth to the absorption linewidth in the (usual) case that this ratio is greater than unity. As the laser intensity is increased, an increasing fraction of the centers are excited into the $\nu=1$ level and the absorption consequently bleaches. This effect can be clearly seen in Fig. 2, which shows the 1.7 K transmission spectra of KBr:SH⁻ at two different incident intensities, measured by tuning the dye-laser grating. The maximum obtainable laser intensities are near the damage threshold of the crystals and destruction of the samples occasionally occurred.

Note that, at high incident laser intensities, nonradiative relaxation can result in a substantial transient heating of the pumped volume of a crystal. From the known T^3 heat capac-

TABLE I. Parameters for the indicated systems: fundamental vibrational peak frequencies, ν_{01} , deconvolved FWHM, γ_{abs} , and fundamental librational sideband peak frequencies, ν_{lib} , of the most abundant isotope at 1.7 K; integrated fundamental vibrational absorption cross sections, σ_{int} , and low-temperature molecular equilibrium orientations.

System	ν_{01} (cm ⁻¹)	γ_{abs} (cm ⁻¹)	σ_{int} (10 ⁻¹⁸ cm)	ν_{lib} (cm ⁻¹)	Orientation
KCl:OH ⁻	3642.11 ^a	0.11 ^a	3.2 ^b	298 ^c	$\langle 100 \rangle^d$
KBr:OH ⁻	3617.47 ^a	0.12 ^a	2.4 ^b	310 ^c	$\langle 100 \rangle^d$
RbCl:OH ⁻	3633.15 ^a	0.13 ^a	3.8 ^b	270 ^a	$\langle 100 \rangle^d$
KCl:OD ⁻	2684.82 ^a	0.10 ^a	0.9 ^b	232 ^c	$\langle 100 \rangle^{d,e}$
KCl:SH ⁻	2591.28 ^a	0.085 ^a	1.8 ^f	370 ^a	$\langle 111 \rangle^g$
KBr:SH ⁻	2575.88 ^a	0.085 ^a	2.3 ^f	332 ^a	$\langle 111 \rangle^g$
KI:SH ⁻	2558.94 ^a	0.028 ^a	1.7	289 ^a	$\langle 111 \rangle^g$
RbCl:SH ⁻	2590.64 ^a	0.090 ^a	2.2 ^f	340 ^a	$\langle 111 \rangle^{h,i}$
RbI:SH ⁻	2563.68 ^a	0.015 ^a	3.3 ^{fj}	266 ^a	$\langle 111 \rangle^h$
CsI:SH ⁻	2535.32 ^a	0.030 ^a	2.3	311 ^a	$\langle 100 \rangle^{f,i}$
KBr:TeH ⁻	2023.55 ^k	0.085 ^k	3.8 ^{k,l}	316 ^a	$\langle 111 \rangle^{h,i}$

^aReference 20.

^bB. Wedding and M. V. Klein, Phys. Rev. **177**, 1274 (1969).

^cReference 18.

^dH. Härtel, Phys. Status Solidi **42**, 369 (1970).

^eAssumed to be isotope independent.

^fReference 19.

^gW. Kuch and U. Dürr, J. Phys. Chem. Solids **42**, 677 (1981).

^hJ. Otto, Phys. Status Solidi B **151**, 363 (1989).

ⁱAssumed from results for similar hosts.

^jApproximated by the corresponding value for RbBr:SH⁻.

^kReference 29.

^lApproximated by the corresponding value for KCl:TeH⁻.

ity of the alkali halides at low temperatures,²⁵ the temperature rise of the focal volume of a sample can be found by integration, assuming that all of the absorbed pump energy is converted into heat. Starting from 1.7 K, the final temperature at the highest intensities for a sample of KBr:SH⁻, say, is found to be 32 K. (Note that the phonons only travel about 15 μm in 6 ns, so that the heat is temporarily confined to the pumped volume.) However, at 32 K the homogeneous width is still small compared to the laser bandwidth and this transient temperature rise is thus found to have a negligible effect upon the fitted lifetime²⁶ (cf. Sec. IV B below).

B. Spectroscopic summary of the investigated samples

Incoherent saturation data can only be interpreted for samples which are well characterized spectroscopically. A number of relevant parameters have been collected together and summarized in Table I for the crystals studied in this paper. The integrated absorption cross sections of SH⁻ in KI and CsI were determined by averaging the results of a chemical analysis technique²⁴ for three different samples each. The corresponding values in the chlorides and bromides have been previously determined photometrically by Otto.¹⁹ Note, however, that the integrated cross section is equal to the vibrational absorption strength divided by the actual dopant concentration, and the relevant strength is found by integrating over the vibrational line *plus all of its sidebands*. Otto appears not to have included the sidebands in his integrations, leading to gross underestimates in the case of the ce-

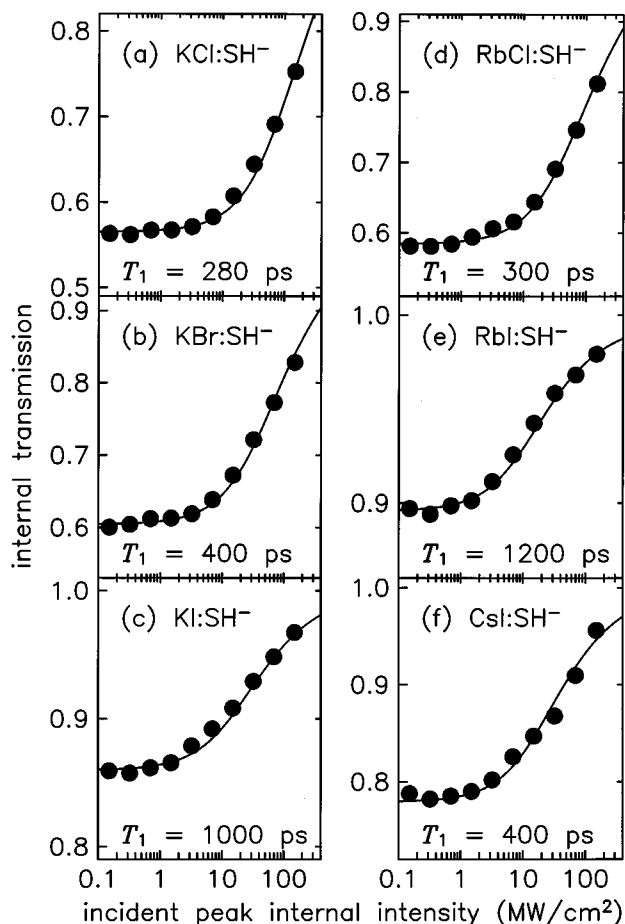


FIG. 3. Saturation data (filled circles) at 1.7 K for nominally (a) KCl+100 ppm SH⁻, (b) KBr+100 ppm SH⁻, (c) KI+60 ppm SH⁻, (d) RbCl+100 ppm SH⁻, (e) RbI+75 ppm SH⁻ and (f) CsI+75 ppm SH⁻. The continuous curves are fits to a rate-equation analysis, giving the values of T_1 listed in each panel.

sium halides. The corresponding errors in the case of the sodium-chloride-structure hosts are much smaller, owing to the weakness of the sidebands, and have been neglected in Table I. The experimental uncertainties in the cross sections of SH⁻ in the table are estimated as $\pm 20\%$.

C. Saturation results

1. SH⁻

In Figs. 3(a)–(c), saturation data (averaged over ~ 200 laser shots per data point) are plotted as the filled circles for SH⁻ in three different potassium halide crystals. The continuous curves are rate-equation fits, as explained in the Appendix, and give the values of the energy relaxation times, T_1 , listed in the figures. (The uncertainties in the lifetimes due to random errors are estimated to be on the order of $\pm 25\%$, judging by the reproducibility of the measurements and the error bars in the fits for a given sample. In addition, however, systematic errors may be introduced by uncertainties in the values of the various laser and sample parameters, notably the cross sections and laser modal structure.) A systematic increase in T_1 as one proceeds from KCl to KI is

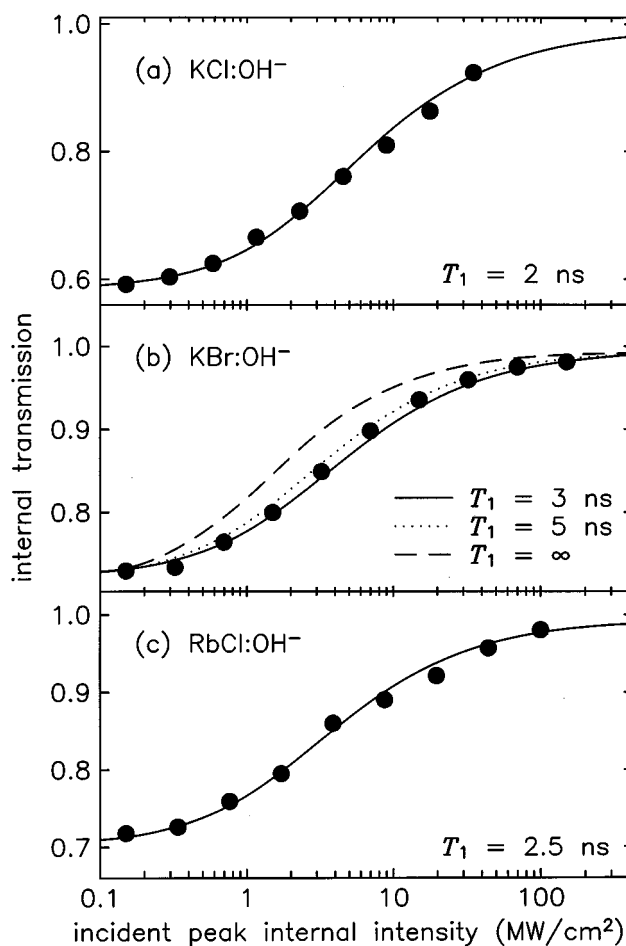


FIG. 4. Saturation data (filled circles) at 1.7 K for nominally (a) KCl+100 ppm OH⁻, (b) KBr+150 ppm OH⁻, and (c) RbCl+700 ppm OH⁻. The curves are fits to a rate-equation analysis, giving the values of T_1 listed in each panel.

evident, visible as a shift in the knee of the curves toward lower intensities. Most importantly, note how short the lifetimes are—a nanosecond or less.

Figures 3(d)–(f) gives the corresponding results for SH⁻ in three rubidium and cesium hosts. Interestingly, the lifetimes for either KCl and RbCl or for KI and RbI are equal to within the $\pm 25\%$ error bars. There appears to be a correlation between the decay times and the lattice constants for the potassium and rubidium hosts: the larger the lattice cage, the slower the rate of relaxation.

On the other hand, the lifetime of SH⁻ in CsI is significantly shorter than that in KI or RbI, despite the fact that CsI has the smallest Debye temperature of all of the hosts studied in this paper. This is one of several indications that a multiphonon-relaxation model²⁷ cannot account for the vibrational decay of the chalcogen hydrides.

2. OH⁻

Turning next to OH⁻, data were collected for three potassium and rubidium hosts, as presented in Fig. 4. Compared to the results for SH⁻ in the same hosts, the hydroxide

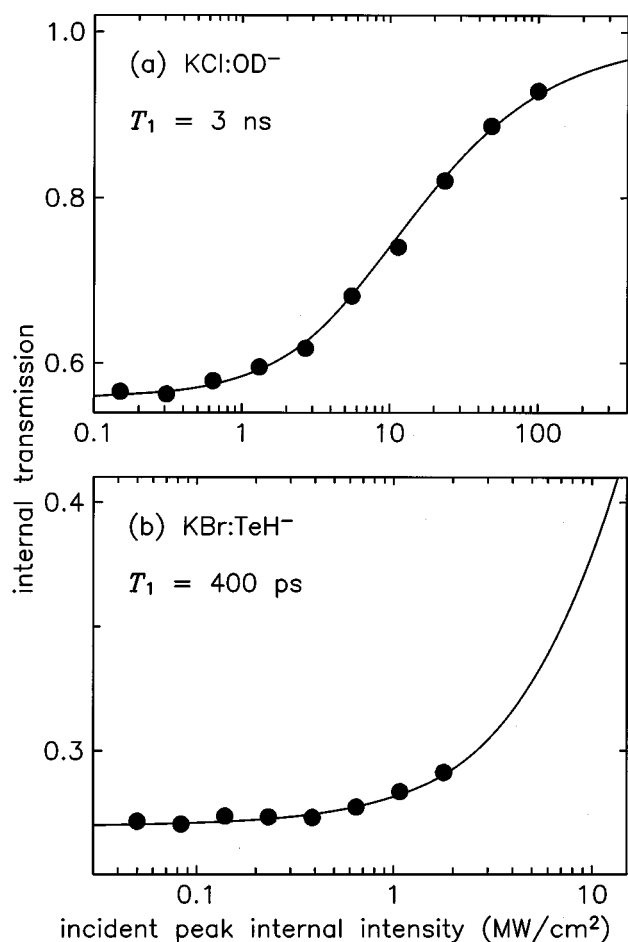


FIG. 5. Saturation data (filled circles) at 1.7 K for (a) KCl+200–250 ppm OD⁻, and (b) KBr+30 ppm TeH⁻. The continuous curves are fits to a rate-equation analysis, giving the values of T_1 listed in each panel.

relaxation times are almost exactly 1 order of magnitude larger. In fact, the times are beginning to approach the limit imposed by the 6 ns laser pulse width. This can be seen most clearly in the case of KBr:OH⁻, the longest lived molecule studied here. The dashed curve in panel (b) shows the predicted transmission when T_1 becomes very long. (Technically, it is assumed to remain shorter than the pulse repetition period of 0.1 s, however.) In this case, the knee in the curve refers no longer to T_1 but instead to the pulse width. Although saturation occurs even at the lowest intensities, the absorption cross section is too small to probe this: Each molecule is visited at most once by a photon. Fortunately, we appear to be safely below this experimental limit—the dotted curve in the figure sets an upper limit of 5 ns on the lifetime.

3. OD⁻

Figure 5(a) presents data for KCl:OD⁻. Compared to the results for KCl:OH⁻ in Fig. 4(a), the OD⁻ relaxation time is slightly increased. Deuterated molecules other than OD⁻ lie at wavelengths greater than 5 μm , outside of the tuning range of the laser system. However, picosecond pump–probe

TABLE II. Summary at 1.7 K of the fitted values of T_1 and of the ratios of the vibrational and librational frequencies.

Impurity	Host	T_1 (ps)	$\nu_{01}/\nu_{\text{lib}}$
SH ⁻ in:	KCl	275	7.0
	KBr	400	7.8
	KI	1000	8.9
	RbCl	300	7.6
	RbI	1200	9.6
OH ⁻ in:	CsI	400	8.2
	KCl	2000	12.2
	KBr	3000	11.7
OD ⁻ in:	RbCl	2500	13.5
TeH ⁻ in:	KCl	3000	11.6
	KBr	400	6.4

experiments of SH and SD in a chalcogenide glass also indicate a slightly increased lifetime for the deuterated species.²⁸

4. TeH⁻

Figure 5(b) presents saturation measurements for KBr:TeH⁻. The maximum laser intensity is rather low, due to the difficulty in accessing the necessary long wavelength. Nevertheless, the TeH⁻ lifetime is on the small end of the range of values measured in this paper and is comparable to the value estimated by simply assuming that the absorption line is lifetime broadened.²⁹

III. VIBRATIONAL RELAXATION MODELS

A. Decay into phonons

The vibrational relaxation times of the hydrated diatomics, as summarized in Table II, show an approximate correlation between vibrational frequency and relaxation rate: The rate tends to increase as the frequency declines. This is qualitatively the expected trend for relaxation into phonons. However, a multiphonon relaxation model can be ruled out for several reasons, of which the two most important ones will be reviewed here.

First, the time scale is completely wrong. Previous studies of the phonon relaxation of CN⁻ in the alkali halides indicated low-temperature lifetimes in the microsecond to millisecond range.⁸ But OH⁻ and SH⁻ have larger vibrational frequencies than CN⁻ and thus slower relaxation would be expected for them—unless, of course, the vibration–phonon coupling strengths are substantially larger for the hydrides. It can be shown¹² that this is not the case by comparing the strengths of the phonon sidebands of the vibrational modes for the two classes of defects—compare the normalized strengths for the coupling of KI:CN⁻ and KI:SH⁻ to bulk phonons in Table III. After accounting for both the increased coupling constant and order of the multiphonon decay, it is found that the nonradiative decay time of KI:SH⁻ should be $\sim 40\%$ larger than that of KI:CN⁻, in striking contrast with experiment.

Second, consider the OD⁻ saturation result. If bulk or localized translational phonons constituted the dominant accepting modes, one would predict a large isotope effect for

TABLE III. Comparison of the integrated sideband strengths of various possible accepting modes for representative diatomic-doped systems of interest in this paper. The sidebands were normalized by multiplying by the cube of the frequency shift from the main vibrational line and dividing by the dopant concentration (as determined from the cross sections given in Table I and the RT resolved vibrational absorption spectra) and absolute frequency (Ref. 12).

System	Sideband mode	Normalized strength (10^{-18} cm^{-1})
KI:CN ⁻	Bulk phonons	12
KI:SH ⁻	Bulk phonons	21
AgCl:CN ⁻	High-frequency local phonon	770
KCl:SH ⁻	Libron	270
KI:SH ⁻	Libron	300

the relaxation time, since the phonons have minimal isotope dependence while the stretching mode frequency changes by roughly $\sqrt{2}$. Thus a large change in the order of the decay process would be expected: $\nu_{01}/\nu_{LO} = 17.0$ for KCl:OH⁻ but only 12.5 for KCl:OD⁻, where ν_{LO} is the longitudinal optic phonon frequency³⁰ of KCl. According to the energy gap law,²⁷ OD⁻ should then relax exponentially faster than OH⁻, which contradicts the observed slight *reduction* in its relaxation rate.

B. Decay into reorientational modes

A high frequency ($\sim 300 \text{ cm}^{-1}$) sideband is found in the vibrational spectra of all of the chalcogen hydrides and is identified as a librational mode of the molecule about its center of mass.²⁰ This mode occurs at high frequencies because of the small moments of inertia of the hydrides (essentially determined by the hydrogen mass) and because of their large orientational potential barriers (as evidenced by the fact that high-temperature free-rotor sidebands are not generally observed, in contrast, for example, to the case of cyanide³¹). Given that high-frequency sidebands were seen to shorten the vibrational lifetimes of CN⁻ in the silver and sodium halides,⁸ it seems reasonable to suppose that these high-frequency librational modes are involved in the vibrational relaxation dynamics of the chalcogen hydrides. (Note that recent results^{20,32} suggest that the reorientational potentials of the XH⁻ defects actually support two distinct elastic configurations: a low-temperature librational potential, relevant to the present work, and a high-temperature Debye potential which influences the vibrational relaxational dynamics at temperatures above $\sim 45 \text{ K}$.²⁶)

In the spirit of the energy gap law,³³ the simplest approach is to look for a correlation between the logarithm of the relaxation times, T_1 , and the number of energy accepting modes, $N = \nu_{01}/\nu_{lib}$. This is plotted in Fig. 6 using the data in Table II. A linear trend is evident, as given by

$$T_1 = \tau_0 e^{AN}, \quad (2)$$

(valid since the nonradiative lifetime is much shorter than the radiative one) with fitted values $\tau_0 = 25 \text{ ps}$ and $A = 0.38$. The hypothesis that the decay is into librational modes explains the weak OH⁻/OD⁻ isotope effect for the lifetime: Upon

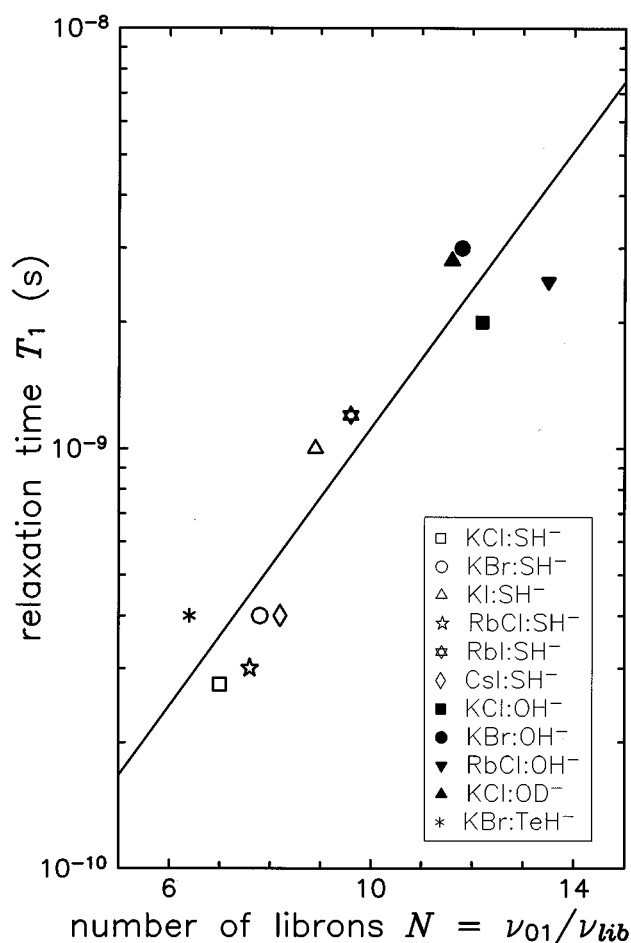


FIG. 6. Vibrational relaxation times of the chalcogen hydrides (symbols) at 1.7 K as a function of the number of energy-matching librational modes, on a semilogarithmic scale. The straight line is a least-squares fit to Eq. (2).

deuterating, both the vibrational and the librational frequencies shift by a factor of approximately $\sqrt{2}$ (from the ratio of reduced masses) and thus N remains unchanged.

In Fig. 6, the vibrational relaxation times are plotted against the accepting number of librational modes. (Technically, one ought to use the FIR librational frequency, which differs in some cases from the sideband frequencies,²⁰ because we are interested in reorientations in the vibrational ground state. However, this frequency is not well known for most of the systems of interest here, and for consistency the sideband values have been used throughout.) This is a naïve view: $N = 10$ would mean that the librational mode has been excited to its 10th harmonic *assuming that such a harmonic exists*. (Not to mention that, because of anharmonicity, the frequency of the n th harmonic is not equal to n times that of the fundamental.)

It is doubtful whether such a high overtone level does in fact exist, as it would imply that the height of the orientational barrier is at least equal to the vibrational frequency of the defect, namely $\sim 2550 \text{ cm}^{-1}$ for SH⁻ and $\sim 3650 \text{ cm}^{-1}$ for OH⁻. The librational frequency of a particular system can be used to estimate the barrier height in the Devonshire model. The Devonshire barrier parameter, K , of a $\langle 111 \rangle$ ori-

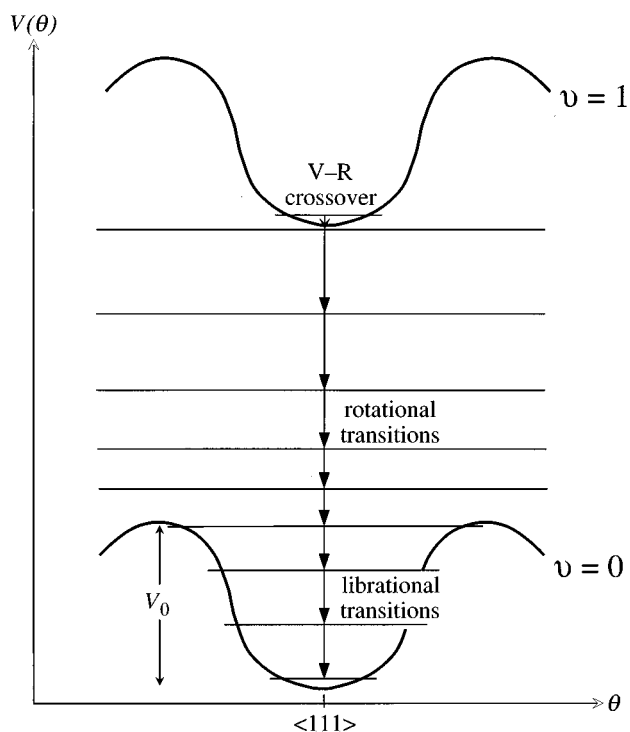


FIG. 7. Schematic diagram of the reorientational relaxation model. The orientational potential surfaces, V , of the ground ($\nu=0$) and excited ($\nu=1$) vibrational manifolds are plotted as a function of one of the two angular coordinates, θ and ϕ . The minima correspond to the low-temperature defect orientations—for example, $\langle 111 \rangle$ for SH^- in the potassium halides. The barrier height, V_0 , between these potential wells varies depending on the angle with which one proceeds away from the minima. A defect which is laser excited into the ground orientational state of the first-excited vibrational manifold relaxes as follows. First, it crosses over into a high rotational level in the ground vibrational manifold, then it cascades down through successive rotational levels at high energies and librational levels at low energies (as indicated by the horizontal line segments). Note that the accepting rotational level is very short lived and hence broad, thus ensuring approximate resonance with the excited vibrational level.

ented defect in a deep well is approximately given by³⁴

$$\nu_{\text{lib}} = \sqrt{40B|K|/3}. \quad (3)$$

Taking³⁵ the diatomic bondlength to be 1.346 Å, the rotational constants, B , of SH^- and SD^- are calculated to be 9.53 and 4.91 cm^{-1} , respectively, neglecting lattice dressing³¹ since we are interested in frequencies well above the host phonon bands. Then, using the values of the librational frequencies of SH^- and SD^- in the potassium halides listed in Table I, one finds $K \approx -900 \text{ cm}^{-1}$. The Devonshire potential has a saddle point at a height of $5/12|K|$ above the bottom of the wells and an absolute maximum at a height of $5/3|K|$, so that the average barrier height is $\sim |K|$. Thus, the librational potential only supports about 3 harmonics.

At higher energies, the diatomics must evidently begin to rotate more and more nearly freely and it is clearly meaningless to speak of the 10th librational level (cf. Fig. 7). Instead, one ought to consider the more general concept of reorientations. Denote the vibrational levels by quantum number ν and the reorientational levels by a label n . The relaxational dynamics occur in two stages:³⁶ A vibration-to-

rotation crossover $|\nu=1, n=0\rangle \rightarrow |\nu=0, n=N\rangle$ into some high reorientational level $|N\rangle$ in the vibrational ground-state manifold, followed by the decay within this manifold $|\nu=0, n=N\rangle \rightarrow |\nu=0, n=0\rangle$. In the current absence of any detailed knowledge of the reorientational potential (in the low-temperature librational configuration), the average reorientational level spacing will be simply taken equal to the fundamental librational frequency.

Any adjacent pair of reorientational levels are strongly coupled by a two- or three-phonon decay process.¹⁸ In particular, the broad linewidth of the libron at 1.7 K (at which temperature, dephasing processes are negligible) implies a decay time of a fraction of a picosecond. Thus the cascading decay of the reorientational excitation $|N\rangle$ to the absolute ground state $|0\rangle$ would be expected to occur in merely a few picoseconds. In that case, the rate-limiting factor in the vibrational relaxation is the crossover process. This, in turn, becomes increasingly less probable as the difference N in the reorientational quantum numbers in the vibrational excited and ground states gets larger and larger—the overlap in the angular part of their wave functions diminishes and it is necessary to go to a higher order of perturbation theory in the interaction Hamiltonian. The overlap integral in the analogous electronic-to-vibrational relaxation problem, for example, is given by Eq. (21) of Ref. 37 and, after making some reasonable assumptions, is found to depend exponentially upon the number of accepting modes. This is similar to Legay's empirical law for vibrational-to-rotational decay.³⁸ In fact, it has been explicitly demonstrated^{39,40} that if both the pumped and accepting reorientational levels are approximated by free-rotor wave functions and a dumb-bell interaction potential restricted to nearest-neighbor forces is assumed, then Fermi's golden rule leads to

$$\frac{1}{T_1} \propto \sum_m \frac{1}{J} e^{-AJ} \cong 2e^{-AJ}, \quad (4)$$

where J is the rotational quantum number of the accepting level given by Eq. (1) above, and where the sum is over the $2J+1$ degenerate m sublevels. Here, the coupling parameter has been written as A , in analogy with Eq. (2) above, and depends logarithmically on J and on the characteristic length for the coupling interaction. It depends implicitly on the degree of hindering of the rotations by the lattice,^{14,17} assisted by mass asymmetry of the defect since the center of mass and the center of interaction then need not coincide.^{40,41}

IV. DISCUSSION

A. Comparison with other OH^- lifetime measurements

The fitted value of T_1 for $\text{KCl}:\text{OH}^-$ in Fig. 4(a) can be compared to previous vibrational fluorescence measurements.⁴² Weak hot vibrational luminescence was detected with an estimated fluorescence quantum efficiency of $\sim 10^{-7}$. The radiative lifetime of the $\text{KCl}:\text{OH}^- \nu=1 \rightarrow 0$ transition is ~ 15 ms, determined from the cross section listed in Table I. This implies $T_1 \approx 1.5$ ns, in unexpectedly good agreement with the saturation result of 2 ns found here.

TABLE IV. Comparison of the absorption, hole burning, and saturation linewidths of SH^- in the indicated hosts at 1.7 K. The absorption FWHM (γ_{abs}) are those of the unmixed hosts. The other two widths refer to crystals which have been double doped with the indicated additional impurities. The homogeneous widths (γ_{homo}) are equal to half of the persistent spectral hole widths, measured in the low-intensity small-burn-time limit (Ref. 45). The lifetime contributions to the homogeneous widths are calculated using the values of T_1 measured by saturation spectroscopy (Ref. 46).

Host	Alloying impurity	γ_{abs} (MHz)	γ_{homo} (MHz)	$(2\pi T_1)^{-1}$ (MHz)
KI	2% KBr	840	640	230
CsI	2% RbI	900	430	270

Picosecond pump-probe measurements⁴³ of $F_H(\text{OH}^-)$ centers in KBr at low temperatures indicate that conversion between two different kinds of orientationally pinned centers occurs, where the OH^- molecular axis is aligned either parallel or perpendicular to the line joining the hydroxide lattice site to that of the F center. One of several possible interpretations is that the electronic energy of the F center is partly transferred to vibrational energy of the OH^- ion, and that this ion subsequently relaxes rotationally, leading to the observed interconversion. Remarkably, the vibrational lifetime of aggregated OH^- centers in KBr is only a factor of ~ 3 larger than what we have measured here for the isolated centers in the same host, suggesting that the F center only weakly perturbs the OH^- relaxation.⁴⁴

B. Comparison with persistent spectral hole burning results

Previous combined hole burning and saturation measurements²³ of ReO_4^- in mixed-alkali-halide crystals indicated that, at liquid helium temperatures, pure dephasing of the vibrational modes by phonons is negligible, so that the hole widths are determined by the relaxation times, T_1 . It is therefore of interest to compare the present saturation measurements with previous hole burning experiments⁴⁵ for SH^- in two mixed crystals, KI+2% KBr and CsI+2% RbI, to see if the same holds true here. No center-frequency dependence of the hole widths was found in the ReO_4^- study. In like fashion, the relaxation time of SH^- in the KI+2% KBr sample does not depend on the absorption peak which is saturated.⁴⁶ Therefore, it seems valid to refer to *the* value of T_1 and of T_2 for a given sample, without regard for the specific homogeneous transition in question. In Table IV, the widths implied by these two times are compared. As well, the ir absorption linewidth for SH^- in the pure crystal corresponding to the dominant component of each mixture is tabulated. The dependence of T_1 on host mixing is small.⁴⁶ If the same is true for T_2 , then it is reasonable to make comparisons with the pure-host ir widths. (The absorption lines of the mixed samples are, of course, inhomogeneously broadened and hence their widths convey no useful dynamical information.) The physical restrictions on the widths in Table IV are

$$\gamma_{\text{abs}} \geq \gamma_{\text{homo}} \geq (2\pi T_1)^{-1}, \quad (5)$$

which one can see are obeyed. In fact, the three quantities are similar in value to each other. The difference between γ_{abs} and γ_{homo} reflects a small amount of inhomogeneous broadening of the unmixed crystals. On the other hand, the difference between γ_{homo} and $(2\pi T_1)^{-1}$ suggests that there may be a pure dephasing contribution to the homogeneous width, as given by T_2^* . Although T_1 controls T_2 at low temperatures³⁰ since T_2^* falls off as T^7 , at our highest laser intensities transient heating of the sample to as much as ~ 35 K is calculated, relaxing this constraint.

Therefore, the homogeneous line may not be lifetime broadened. To check that this does not alter the fits to T_1 in the saturation analysis, we set $T_2 = 500$ ps for SH^- in KI+2% KBr (deduced from the homogeneous width in Table IV and $T_1 = 700$ ps (from the saturation fit in Ref. 46, obtained assuming lifetime broadening of the homogeneous line) and reran the saturation analysis. The resulting theoretical curves were found to be virtually unchanged.

There is an interesting connection between the role of molecular reorientations in the vibrational relaxation and in the persistent spectral hole burning. It has been proposed here that the vibration of the diatomic relaxes by coupling to an approximately resonant orientational level in the vibrational ground state manifold, presumably one which is so high in energy that it constitutes a nearly free rotation. The molecule subsequently relaxes by phonon-mediated cascading from one rotational level to another and rotates during this time. Gradually, the reorientations become hindered, until finally the molecule becomes trapped in some particular potential well, most likely different in orientation and in vibrational frequency than that before excitation. This would simultaneously explain both the transient and persistent molecular dynamics.

C. Comparison with vibrational relaxation rates of other systems

Table V lists decay times and orders for nonradiative vibrational relaxation into predominantly bulk phonons, local translations, or reorientations of a number of impurity systems. For the diatomic-doped rare-gas matrices, the order of the reorientational decay processes have been calculated using Eq. (1), taking the values of the rotational constants in the appropriate electronic states of OH, NH, and HCl from Table 39 of Ref. 47. In the case of CH_3F , the indicated relaxation is for ν_3 , the lowest frequency vibrational mode, so that relaxation into lower energy internal vibrational levels is not possible, and the order is calculated assuming rotations about the figure axis of the molecule.

A good correlation for all of the systems, in the bulk and local phonon cases, is found between the lifetimes and the number of accepting modes, remembering that radiative decay dominates when the order becomes too large. On the other hand, for reorientational decay, it appears that molecules in ionic hosts relax much faster than those in van der Waals hosts of equal decay order, which suggests that Coulombic forces increase the V - R coupling strength.

This, however, cannot be the whole story, because

TABLE V. Comparison of the low-temperature, low-concentration, $1 \rightarrow 0$ vibrational relaxation times of the indicated systems. The order of the decay process is listed in the third column (those denoted by an asterisk refer to vibrational relaxation within an excited electronic manifold).

System	Lifetime	Order	Reference
Coupling to local/ bulk phonons			
Se_2^- in KCl	~ 2.5 ps	2	Mungan <i>et al.</i> ^a
O_2^- in KCl, NaCl	30–40 ps	3*	Bürger <i>et al.</i> ^b
CN^- in Ag, Na halides	50–700 μs	7–8	Happek <i>et al.</i> ^c
CN^- in K, Rb, Cs halides	6–50 ms	10–25	Happek <i>et al.</i> ^c
CO, NO in Ne, Ar	15–30 ms	30–50	Dubost <i>et al.</i> ^d
Coupling to reorientations			
SH^- , TeH^- in alkali halides	300–1200 ps	7–10	This work
OH^- , OD^- in alkali halides	2–3 ns	12–14	This work
OH in Ne	10 μs	13*	Brus <i>et al.</i> ^e
CH_3F in Ne, Ar, Kr, Xe	3–60 μs	14	Abouaf-Marguin <i>et al.</i> ^f
NH in Ar	200 μs	14	Bondybey ^g
HCl in Ar, Kr, Xe	1 ms	16	Young <i>et al.</i> ^h

^aC. E. Mungan, Ph.D. thesis, Cornell University, 1995 (unpublished).

^bA. Bürger, C. Krysch, L. O. Schwan, and D. Schmid, *J. Lumin.* **58**, 287 (1994).

^cReference 8.

^dReferences 2 and 3.

^eReference 13.

^fReference 41.

^gReference 6.

^hReference 17.

CN^- is also an ionic system. The low-temperature vibrational decay times of the chalcogen hydrides are compared to those of cyanide doped in salt crystals in Fig. 8, by combining Fig. 6 above with Fig. 3(a) of Ref. 8. The continuous curves are fits to energy gap laws for the nonradiative parts of the relaxation. The prefactor, τ_0 in Eq. (2), only differs by a factor of 2 for the two sets of systems, being equal to 50 ps for CN^- and 25 ps for XH^- . This near agreement is probably fortuitous, in light of the complicated dependence of this factor on a large number of host and impurity parameters.^{27,40} Be that as it may, the two curves thus extrapolate back to almost the same point on the vertical axis for zero accepting modes, and the $\sim 10^6$ difference in times for CN^- in the silver or sodium halides compared to SH^- in the alkali halides (both of which have about the same decay order) is due entirely to the exponential coefficient, $A = 1.93$ for CN^- and 0.38 for XH^- . The difference between these two values can be used to find the ratio of the coupling parameters to the local translational and librational modes. Modeling the density of states of these modes using the Einstein approximation and assuming that the number density of librational (translational) modes is equal to 2 (3) per impurity molecule based on their angular (spatial) degeneracies, we have $\Delta(\text{XH}^-)/\Delta(\text{CN}^-) = 2.7$, where Δ is the coupling parameter defined by Ref. 27 which does not include, however, Coulombic terms in the interaction potential.

To compare this to experiment, the high-frequency local-phonon sideband of $\text{AgCl}:\text{CN}^-$ and the librational sideband of $\text{KCl}:\text{SH}^-$ at 1.7 K are normalized and their strengths in-

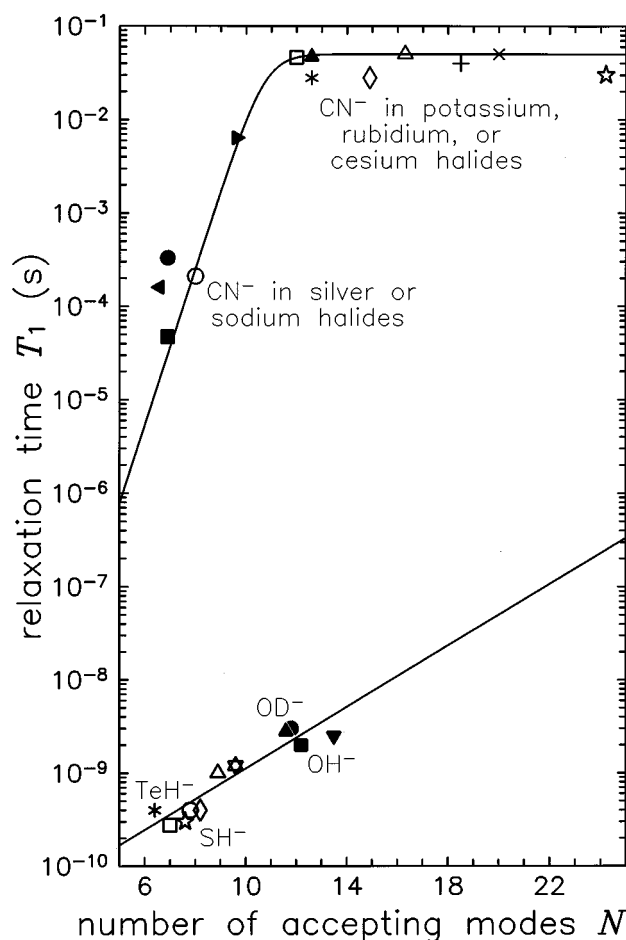


FIG. 8. Comparison of the $1 \rightarrow 0$ vibrational relaxation times (symbols) of CN^- and of XH^-/XD^- in the alkali and silver halides at 1.7 K. For clarity, the symbol legends are not reproduced, since they are identical to those of Fig. 3(a) of Ref. 8 for cyanide and to Fig. 6 for the hydrides, from which figures the solid curves are also taken. The abscissa gives the ratio of the vibrational frequency to the accepting mode frequency, defined to be the longitudinal optic phonon frequency for CN^- in the potassium, rubidium, and cesium halides, the highest frequency localized translational mode in the case of CN^- in the silver and sodium halides, and the librational frequency for the chalcogen hydrides.

tegrated, giving 270 cm^{-1} for the $\text{KCl}:\text{SH}^-$ librational mode and 770 cm^{-1} for the $\text{AgCl}:\text{CN}^-$ translational sideband (cf. Table III), in the opposite ratio to what is predicted. As a check that these values are really representative of the whole class of molecules, the normalized coupling strength of $\text{KI}:\text{SH}^-$ to librations is also evaluated and can be seen from Table III to agree to within 10% with that of $\text{KCl}:\text{SH}^-$. Thus the enhanced coupling of the vibrational modes to librations as compared to translations is not easily explained. On the other hand, in Ref. 8, the coupling of $\text{AgCl}:\text{CN}^-$ to its high-frequency local phonons and of $\text{KI}:\text{CN}^-$ to bulk phonons was found to be the same, in striking contrast to the huge difference in sideband strengths listed in Table III. Hence, it is not just the XH^- systems whose coupling parameters are not related in the expected manner to the sideband strengths. Furthermore, it does not seem credible that the striking difference between the lifetimes of the XH^- impurities and the

other systems listed in Table V can be neatly swept into the exponential coupling coefficient in this way, because all of the latter systems show much less variation in the ratios of the decay order and the logarithm of the lifetime. Evidently, there is something unique about the ionic hydrides, and a theoretical explanation must be sought with this clearly in mind.

V. SUMMARY

Incoherent saturation measurements of OH^- , OD^- , SH^- , and TeH^- in the alkali halides at 1.7 K reveal that the fundamental vibrational lifetimes vary between 0.3 and 3 ns in the electronic ground state. These times are too short to be explained using a multiphonon-relaxation model, by comparison to the equal-order decays of CN^- into local and bulk phonons.⁸ Furthermore, such a model predicts a large OH^-/OD^- isotope effect in the relaxation rate, which is contradicted by experiment.

On the other hand, a strong correlation is discovered between the vibrational relaxation times and the librational sidebands observed by ir spectroscopy. This correlation can be quantified in terms of an energy gap law for the decay of the excited vibrational level into an appropriate number of reorientational modes. Convincingly, this model predicts a null isotope effect upon deuteration, in agreement with the experimental data. Furthermore, persistent hole burning measurements in mixed crystals are consistent with a picture in which a vibrationally excited defect reorients during relaxation.⁴⁵ However, an accurate model describing the vibration-to-rotation transfer cannot be constructed until the reorientational potential is better understood.

The OH^- lifetimes measured here are consistent with that deduced from hot vibrational luminescence observations of the isolated molecule in KCl.⁴² They are also compatible with the observed interconversion between red- and blue-shifted $F_H(\text{OH}^-)$ centers in KBr, though it is not yet fully clear how the $\langle 200 \rangle$ -neighboring F center perturbs the OH^- reorientational potential.^{44,48}

The dramatically smaller lifetimes of the XH^- impurities in alkali halides compared to those⁸ of CN^- in the same hosts at the same low temperatures and concentrations could be explained by postulating a factor of ~ 3 change in the coupling parameters. However, direct spectroscopic measurements of the relevant sideband strengths do not support such a hypothesis.

A large jump in the relaxation rates is also found when one compares the equal-order vibrational decay of diatomic hydrides in ionic and van der Waals hosts. For example, the systems $\text{KCl}:\text{SH}^-$ and $\text{Ar}:\text{HCl}$ are isoelectronic and the mass asymmetries and rotational constants of the two guest molecules are similar. Nevertheless, SH^- decays in picoseconds, while the relaxation of HCl is within an order of magnitude of its radiative limit.⁵ Apparently, Coulombic forces significantly strengthen the $V-R$ coupling.

ACKNOWLEDGMENTS

We thank R. O. Pohl, C. R. Pollock, and M. V. Klein for the OH^- and OD^- samples used in this study. Communications with R. H. Silsbee, S. A. FitzGerald, J. Tu, and V. Elser have been helpful. Retrieval of archived computer files by S. R. Bickham is also acknowledged. This work has been supported in part by NSF-DMR-9631298, ARO-DAAH04-96-1-0029, and NASA-NAGW-2768.

APPENDIX: ANALYSIS OF INCOHERENT SATURATION DATA

As discussed in Secs. 2.7 and 2.14 of Ref. 22, the use of rate equations is appropriate provided that the laser bandwidth is much larger than the lifetime-limited linewidth, $(2\pi T_1)^{-1}$, as is always true in the present experiments. In that case, one recovers the Einstein limit of the optical Bloch equations because the Rabi oscillations of centers having different detunings interfere, masking any coherent effects. However, standard expressions such as Eq. (6.20) of Ref. 21 cannot be used here for several reasons: Steady state may not be fully attained because of the short temporal width of the laser pulses, many of the samples are intermediate between the homogeneous and strongly inhomogeneous broadening regimes, and the laser pulse has non-negligible spatial and spectral variations. So instead, the rate equations are numerically integrated.

An incident laser pulse is split into temporal, spectral, and radial bins and each piece thereof is propagated through the crystal, which is itself subdivided into longitudinal bins. The absorption spectrum is resolved into its component homogeneous lines lying within the laser bandwidth, and, when necessary, the inequivalent molecular orientations are distinguished. Each piece of the pulse interacts with homogeneous peak i at longitudinal position z , radius r , and time t according to the rate equation

$$\dot{N}_{2i}(z,r,t) = \Delta N_i(z,r,t) \int \frac{\sigma_i(\nu) dI(z,r,t,\nu)}{hc\nu} - \frac{N_{2i}(z,r,t)}{T_1}, \quad (\text{A1})$$

where N_{1i} and N_{2i} are the ground- and excited-state populations of transition i , having constant total population N_i and difference $\Delta N_i \equiv N_{1i} - N_{2i}$, and $\sigma_i(\nu)$ is the absorption cross section of this transition (with frequency, ν , expressed in wave numbers). The first term on the right-hand side of this equation represents the difference between the rates of stimulated emission and absorption, and the last term results from spontaneous decay with rate $1/T_1$, which is assumed to be constant for all centers lying within the 0.27 cm^{-1} laser bandwidth. Next, N_{2i} is rewritten as $(N_i - \Delta N_i)/2$ and substituted on both sides, and the time derivative of $\Delta N_i(t)$ is approximated by $[\Delta N_i(t + \Delta t) - \Delta N_i(t)]/\Delta t$. Suppressing the dependences on z and r , Eq. (A1) becomes

$$\Delta N_i(t+\Delta t) = \Delta N_i(t) \left[1 - 2\Delta t \int \sigma_i(\nu) \frac{dI(t, \nu)}{hc\nu} \right] + \frac{\Delta t}{T_1} [N_i - \Delta N_i(t)], \quad (\text{A2})$$

which is an initial value problem with $\Delta N_i(0) = N_i$. The integral is numerically approximated by

$$\int \sigma_i(\nu) \frac{dI(t, \nu)}{hc\nu} \cong \sum_{j=1}^M \sigma_i(\nu_j) \frac{\Delta I(t, \nu_j)}{hc\nu_j}, \quad (\text{A3})$$

i.e., M frequency bins of width $\Delta\nu$ centered at ν_j for bin j . Assuming Gaussian temporal, spectral, and radial (at the focus) profiles, the intensity of each portion of the incident laser pulse is given by

$$\Delta I(z=0, r, t, \nu) = I_{\text{peak}} \frac{\Delta\nu}{\sqrt{2\pi}\sigma_\nu} \exp\left[-\frac{(t-t_0)^2}{2\sigma_t^2}\right] \times \exp\left[-\frac{r^2}{2\sigma_r^2}\right] \exp\left[-\frac{(\nu-\nu_{01})^2}{2\sigma_\nu^2}\right], \quad (\text{A4})$$

where $z=0$ indicates the front surface of the sample. The Gaussian sigmas are related in an obvious way to the temporal ($\Delta t_{\text{las}} = 6$ ns), spectral ($\Delta\nu_{\text{las}} = 0.27$ cm⁻¹), and focal ($\Delta r_{\text{foc}} \approx 100$ μm) FWHM. In this expression, the laser is assumed to have been tuned into resonance with the sample's absorption peak frequency ν_{01} , and I_{peak} is the incident peak internal intensity which appears on the abscissae of all the saturation curves. Experimentally, $I_{\text{peak}} = bE(\Delta t_{\text{las}})^{-1}(\Delta r_{\text{foc}})^{-2}$, where E is the reflection-corrected total pulse energy measured using an energy meter, and b is a numerical factor equal to $(4 \ln 2/\pi)^{3/2} = 0.83$.

Subsequently, suppressing the dependences on r and t , ΔI is obtained from the recursion relation

$$\Delta I(z+\Delta z, \nu) = \Delta I(z, \nu) e^{-\Delta z \alpha(z, \nu)}, \quad \text{where}$$

$$\alpha(z, \nu) = \sum_i \Delta N_i(z) \sigma_i(\nu), \quad (\text{A5})$$

with ΔN_i given by Eq. (A2). Assuming that the integrated cross section is constant and equal to σ_{int} for all centers lying within the laser bandwidth, it then follows that

$$\sigma_i(\nu) = \frac{\sigma_{\text{int}}}{\pi} \frac{\gamma_{\text{homo}}/2}{(\nu-\nu_i)^2 + (\gamma_{\text{homo}}/2)^2}. \quad (\text{A6})$$

At low temperatures, the homogeneous lines are presumed to be lifetime broadened; in general however, their width, γ_{homo} , may also depend on T_2^* , the pure dephasing time.

All that is left is to find N_i . The fractional number of centers i composing the absorption band is equal to the ratio of the homogeneous strength of transition i to the entire ir strength, S_{01} . Making the standard assumption that the homogeneous centers are log-normal distributed, it is then apparent that

$$N_i = \frac{S_{01}}{\sigma_{\text{int}}} \frac{\exp\left[-\frac{(\nu_i - \nu_{01})^2}{2\sigma^2}\right]}{\sum_i \exp\left[-\frac{(\nu_i - \nu_{01})^2}{2\sigma^2}\right]}, \quad (\text{A7})$$

where σ defines the width of the inhomogeneous distribution. It is not necessary to measure S_{01} separately, as it can be deduced from the value of the low-intensity, unsaturated transmission. For a very inhomogeneous line, σ is determined by the absorption linewidth, γ_{abs} . In most cases, however, the line is nearly homogeneous and a Voigt line shape is appropriate. Defining $\nu_{1/2} \equiv \nu_{01} - \frac{1}{2}\gamma_{\text{abs}}$, the distribution width is implicitly given by the following relation.

$$\frac{1}{2} \sum_i \frac{\exp\left[-\frac{(\nu_i - \nu_{01})^2}{2\sigma^2}\right]}{(\nu_i - \nu_{01})^2 + (\gamma_{\text{homo}}/2)^2} = \sum_i \frac{\exp\left[-\frac{(\nu_i - \nu_{01})^2}{2\sigma^2}\right]}{(\nu_i - \nu_{1/2})^2 + (\gamma_{\text{homo}}/2)^2}. \quad (\text{A8})$$

If the absorption spectrum consists of multiple overlapping bands, σ must be determined separately for each of them.

The final step consists in calculating the transmission. For consistency, this is done by explicitly summing over the bins (note that the radial bins must be multiplied by the radial coordinate in the cylindrical integral) both before and after propagation of the laser pulse across the sample. The internal transmission is the ratio of these two numbers.

It is generally necessary to take into account the orientations of the molecular centers relative to the laser polarization. Let this polarization direction define the y axis and focus attention on a dipole pointing at an angle θ with respect to this axis. The transition strength is proportional to the square of the component of the dipole matrix element in the direction of the electric field vector. That is, one could define an integrated absorption cross section for this single molecule as $\sigma_{\text{int}}^{(\theta)}$, with $\sigma_{\text{int}}^{(\theta)} \propto \cos^2 \theta$. But one must recover the spectroscopic value σ_{int} upon averaging over a macroscopic number of centers, which implies

$$\sigma_{\text{int}}^{(\theta)} = 3\sigma_{\text{int}} \cos^2 \theta \quad (\text{A9})$$

for a cubic crystal. Let the fractional number of centers having orientation θ be denoted $N_i^{(\theta)}/N_i$. For example, suppose the laser polarization is [100]. Then for $\langle 100 \rangle$ centers, one-third of them are parallel ($\theta=0^\circ$) to the field and experience a factor of 3 enhancement in their cross section, while the other two-thirds are orthogonal and do not couple to the laser light at all. In the case of $\langle 111 \rangle$ orientations and the same [100] polarization, all centers are equivalent with $\theta = \cos^{-1}(1/\sqrt{3})$, so that $3 \cos^2 \theta = 1$ and there is no enhancement. Finally, for $\langle 110 \rangle$ molecules, two-thirds of them have $\theta=45^\circ$ which gives an enhancement factor of 1.5 and the other one-third are orthogonal. If the centers are randomly oriented with respect to the electric field and angular bins of width $\Delta\theta$ are defined, the number of molecules of transition i in the bin having mean orientation θ is $N_i^{(\theta)} = N_i \Delta\theta \sin \theta$. The saturation analysis then consists in replacing N_i and σ_{int} by $N_i^{(\theta)}$ and $\sigma_{\text{int}}^{(\theta)}$, respectively, and keeping track of both i and θ .

The computation proceeds by defining the necessary grid of bins and performing the numerical integration and pulse propagation steps. Numerous checks have been performed to ensure that the calculations have been done properly, such as observing how the results depend on the input parameters and testing to see that the grid resolution is small enough to prevent sizable discretization and round-off errors.

In this way, the theoretical saturation curves in Sec. II C were obtained. The values of T_1 were varied by trial and error until the curves fit the data as well as possible, judging by eye.

- ¹H. Dubost, L. Abouaf-Marguin, and F. Legay, *Phys. Rev. Lett.* **29**, 145 (1972).
- ²H. Dubost and R. Charneau, *Chem. Phys.* **12**, 407 (1976).
- ³I. Hadj Bachir, R. Charneau, and H. Dubost, *Chem. Phys.* **177**, 675 (1993).
- ⁴V. E. Bondybey and A. Nitzan, *Phys. Rev. Lett.* **38**, 889 (1977).
- ⁵J. M. Wiesenfeld and C. B. Moore, *J. Chem. Phys.* **70**, 930 (1979).
- ⁶V. E. Bondybey, *J. Chem. Phys.* **65**, 5138 (1976).
- ⁷Y. Yang and F. Lüty, *Phys. Rev. Lett.* **51**, 419 (1983).
- ⁸U. Happek, C. E. Mungan, W. von der Osten, and A. J. Sievers, *Phys. Rev. Lett.* **72**, 3903 (1994).
- ⁹R. W. Tkach, T. R. Gosnell, and A. J. Sievers, *Opt. Lett.* **9**, 122 (1984).
- ¹⁰H. Dubost, R. Charneau, M. Chergui, and N. Schwentner, *J. Lumin.* **48/49**, 853 (1991).
- ¹¹C. E. Mungan, U. Happek, and A. J. Sievers, *J. Lumin.* **58**, 33 (1994). The lifetimes reported in the present paper are more accurate.
- ¹²C. E. Mungan, U. Happek, J. T. McWhirter, and A. J. Sievers, in *Defects in Insulating Materials*, edited by O. Kanert and J.-M. Spaeth (World Scientific, Singapore, 1993), Vol. 1, p. 536.
- ¹³L. E. Brus and V. E. Bondybey, *J. Chem. Phys.* **63**, 786 (1975).
- ¹⁴V. E. Bondybey and L. E. Brus, *J. Chem. Phys.* **63**, 794 (1975).
- ¹⁵M. T. Bowers and W. H. Flygare, *J. Chem. Phys.* **44**, 1389 (1966).
- ¹⁶H. E. Hallam, in *Vibrational Spectroscopy of Trapped Species*, edited by H. E. Hallam (Wiley-Interscience, London, 1973), p. 67.
- ¹⁷L. Young and C. B. Moore, *J. Chem. Phys.* **81**, 3137 (1984).
- ¹⁸M. V. Klein, B. Wedding, and M. A. Levine, *Phys. Rev.* **180**, 902 (1969).
- ¹⁹J. Otto, *Phys. Status Solidi B* **142**, 105 (1987).
- ²⁰C. E. Mungan, R. Lai, and A. J. Sievers, *Phys. Rev. B* **54**, 9204 (1996).
- ²¹L. Allen and J. H. Eberly, *Optical Resonance and Two-Level Atoms* (Dover, New York, 1987).
- ²²R. Loudon, *The Quantum Theory of Light*, 2nd ed. (Clarendon, Oxford 1990).
- ²³W. E. Moerner, A. R. Chraplyvy, and A. J. Sievers, *Phys. Rev. B* **29**, 6694 (1984).
- ²⁴C.-K. Chi and E. R. Nixon, *J. Phys. Chem. Solids* **33**, 2101 (1972).
- ²⁵N. W. Ashcroft and N. D. Mermin, *Solid State Physics* (Saunders College, Philadelphia, 1976).
- ²⁶C. E. Mungan, R. Lai, and A. J. Sievers, *Chem. Phys. Lett.* **270**, 309 (1997).
- ²⁷A. Nitzan, S. Mukamel, and J. Jortner, *J. Chem. Phys.* **63**, 200 (1975).
- ²⁸J. R. Engholm, C. W. Rella, H. A. Schwettman, and U. Happek, *Phys. Rev. Lett.* **77**, 1302 (1996).
- ²⁹C. E. Mungan, U. Happek, T. Z. Hossain, and A. J. Sievers, *J. Phys. Chem. Solids* **56**, 735 (1995).
- ³⁰A. S. Barker, Jr. and A. J. Sievers, *Rev. Mod. Phys.* **47**, S1 (1975).
- ³¹C. E. Mungan, R. C. Spitzer, J. P. Sethna, and A. J. Sievers, *Phys. Rev. B* **43**, 43 (1991).
- ³²R. Lai, C. E. Mungan, and A. J. Sievers, *Phys. Rev. Lett.* **76**, 1864 (1996).
- ³³R. Englman, *Non-Radiative Decay of Ions and Molecules in Solids* (North-Holland, Amsterdam, 1979).
- ³⁴M. Indere and K.-L. Jüngst, *J. Phys. Chem. Solids* **37**, 1105 (1976).
- ³⁵J. Senekowitsch, H.-J. Werner, P. Rosmus, E.-A. Reinsch, and S. V. O'Neill, *J. Chem. Phys.* **83**, 4661 (1985).
- ³⁶D. J. Diestler, E.-W. Knapp, and H. D. Ladouceur, *J. Chem. Phys.* **68**, 4056 (1978).
- ³⁷Y. Farge, J. M. Ortega, and R. H. Silsbee, *J. Chem. Phys.* **69**, 3972 (1978).
- ³⁸F. Legay, in *Chemical and Biochemical Applications of Lasers*, edited by C. B. Moore (Academic, New York, 1977), Vol. 2, p. 43.
- ³⁹K. F. Freed and H. Metiu, *Chem. Phys. Lett.* **48**, 262 (1977).
- ⁴⁰M. Berkowitz and R. B. Gerber, *Chem. Phys.* **37**, 369 (1979).
- ⁴¹L. Abouaf-Marguin and B. Gauthier-Roy, *Chem. Phys.* **51**, 213 (1980).
- ⁴²K. K. Rebane, P. M. Saari, and T. H. Muring, in *Luminescence of Crystals, Molecules, and Solutions*, edited by F. Williams (Plenum, New York, 1973), p. 690.
- ⁴³M. Leblans, E. Gustin, A. Bouwen, and D. Schoemaker, *J. Lumin.* **58**, 388 (1994).
- ⁴⁴E. Gustin, M. Leblans, A. Bouwen, D. Schoemaker, and F. Lüty, *Phys. Rev. B* **54**, 6963 (1996).
- ⁴⁵C. E. Mungan and A. J. Sievers, *J. Opt. Soc. Am. B* **9**, 746 (1992).
- ⁴⁶C. E. Mungan, U. Happek, J. T. McWhirter, and A. J. Sievers, *Mat. Sci. Forum* **239–241**, 443 (1997).
- ⁴⁷G. Herzberg, *Molecular Spectra and Molecular Structure I. Spectra of Diatomic Molecules*, 2nd ed. (Van Nostrand, New York, 1953).
- ⁴⁸E. Gustin, M. Leblans, A. Bouwen, and D. Schoemaker, *Phys. Rev. B* **54**, 6977 (1996).